J Biomol NMR (2010) 48:1–11
DOI 10.1007/s10858-010-9432-x

ARTICLE

Structure analysis of membrane-reconstituted subunit *c*-ring of *E. coli* H^+-ATP synthase by solid-state NMR

Yasuto Todokoro · Masatoshi Kobayashi · Takeshi Sato · Toru Kawakami · Ikuko Yumen · Saburo Aimoto · Toshimichi Fujiwara · Hideo Akutsu

Received: 14 May 2010 / Accepted: 15 June 2010 / Published online: 2 July 2010

Abstract The subunit *c*-ring of H^+-ATP synthase (F_oc-ring) plays an essential role in the proton translocation across a membrane driven by the electrochemical potential. To understand its structure and function, we have carried out solid-state NMR analysis under magic-angle sample spinning. The uniformly [^{13}C, ^{15}N]-labeled F_oc from *E. coli* (EF_oc) was reconstituted into lipid membranes as oligomers. Its high resolution two- and three-dimensional spectra were obtained, and the ^{13}C and ^{15}N signals were assigned. The obtained chemical shifts suggested that EF_oc takes on a hairpin-type helix-loop-helix structure in membranes as in an organic solution. The results on the magnetization transfer between the EF_oc and deuterated lipids indicated that Ile55, Ala62, Gly69 and F76 were lined up on the outer surface of the oligomer. This is in good agreement with the cross-linking results previously reported by Fillingame and his colleagues. This agreement reveals that the reconstituted EF_oc oligomer takes on a ring structure similar to the intact one in vivo. On the other hand, analysis of the ^{13}C nuclei distance of [3-^{13}C]Ala24 and [4-^{13}C]Asp61 in the F_oc-ring did not agree with the model structures proposed for the EF_oc-decamer and dodecamer. Interestingly, the carboxyl group of the essential Asp61 in the membrane-embedded EF_oc-ring turned out to be protonated as COOH even at neutral pH. The hydrophobic surface of the EF_oc-ring carries relatively short side chains in its central region, which may allow soft and smooth interactions with the hydrocarbon chains of lipids in the liquid-crystalline state.

Keywords Membrane protein · F_o subunit *c* · Specific isotope-labeling · Lipid-protein interaction · Magnetization transfer · Rotational resonance

Abbreviations

EF_oc	H^+-ATP synthase subunit *c* from *E. coli*
TF_oc	H^+-ATP synthase subunit *c* from thermophilic *Bacillus* PS3
IF_oc	Na^+-ATPase subunit *c* from *Ilyobacter tartaricus*
MALDI-TOF MS	Matrix-assisted laser desorption/ ionization time of flight mass spectrometry
Boc	*tert*-Butoxycarbonyl group
ssNMR	Solid-state NMR
MAS	Magic angle sample spinning
RR	Rotational resonance
DARR	Dipole-assisted rotational resonance
RFDR	Radio frequency-driven recoupling

Electronic supplementary material The online version of this article (doi:10.1007/s10858-010-9432-x) contains supplementary material, which is available to authorized users.

Y. Todokoro · M. Kobayashi · T. Sato · T. Kawakami · I. Yumen · S. Aimoto · T. Fujiwara · H. Akutsu (✉)
Institute for Protein Research, Osaka University, 3-2 Yamadaoka, Suita 565-0871, Japan
e-mail: akutsu@protein.osaka-u.ac.jp

H. Akutsu
Department of Biophysics and Chemical Biology, Seoul National University, Kwanak-gu, Seoul, Korea

Present Address:
Y. Todokoro
Yokohama City University, Tsurumi, Yokohama 230-0045, Japan

M. Kobayashi
Sumitomo Rubber Industries, Ltd., Tsutsui-cho, Kobe 651-0071, Japan

CODSHD	^{13}C-NMR observation of ^{2}H-selective ^{1}H-depolarization
TPPM decoupling	Two-pulse phase modulation
FID	Free induction decay

F_1F_o ATP synthase is a ubiquitous molecular motor involved in H^+-mediated energy conversion in organisms from bacteria to man. The H^+-driven ATP synthase transfers the energy of the transmembrane electrochemical potential to ATP. It consists of a water-soluble F_1 sector and a membrane integrated F_o sector. The former has catalytic sites for ATP synthesis/hydrolysis, and the latter mediates H^+ transport across membranes (Boyer 1997; Yoshida et al. 2001; Dimroth et al. 2006). The F_1 and F_o sectors comprise multiple subunits, their compositions being $\alpha_3\beta_3\gamma\delta\varepsilon$ and ab_2c_n, respectively. The *c* subunits form a ring rotor in F_o. This has been extensively studied biochemically and genetically (Hutcheon et al. 2001; Fillingame and Dmitriev 2002; Suzuki et al. 2002; Moore and Fillingame 2008). Furthermore, the ring structures of the yeast (Stock et al. 1999), chloroplast (Vollmar et al. 2009), and cyanobacterial (Pogoryelov et al. 2009) H^+-ATP synthases, and F-type (Meier et al. 2005) and V-type (Murata et al. 2005) Na^+-ATPases from bacteria have been reported. The numbers of the subunits in the rings are 10, 14, 15, 11, and 10, respectively. Each subunit takes on a hairpin structure with two membrane-spanning α-helices. In the F_o complex, the subunit *c*-ring interacts with subunit *a*, in which an acidic amino acid residue in the *c*-ring plays an essential role. The crystal structure around this acidic amino acid residue is different even for the two H^+-translocating *c*-rings (Vollmar et al. 2009; Pogoryelov et al. 2009). In H^+-ATP synthase, protons are assumed to be translocated through subunits *a* and *c* with the involvement of the essential amino acid residue (Moore and Fillingame 2008).

The structure of subunit *c* from *E. coli* (EF_oc) in an organic solvent was determined by NMR analysis (Girvin et al. 1998). In this solvent, a conformational change of its C-terminal helix on deprotonation of the essential residue Asp61 was found (Rastogi and Girvin 1999). A rotation mechanism for the c_{12}-ring (PDB ID 1J7F) driven by the twisting of a helix coupled with H^+-translocation was proposed on the basis of this observation (Rastogi and Girvin 1999; Dmitriev et al. 1999). Later, the structural model was modified to that of a decamer ring (Jiang et al. 2001). On the other hand, the structure of subunit *c* from thermophilic *Bacillus* PS3 (TF_oc) indicated that de-protonation of the essential acidic residue (Glu56) did not induce a large conformational change (Nakano et al. 2006). On the basis of this observation, we proposed a new mechanism. In this, side chain flipping at the essential acidic residue on protonation/deprotonation drives H^+-translocation and the rotation of the *c*-ring in association with the membrane potential (Nakano et al. 2006).

EF_oc is a hydrophobic protein composed of 79 amino acid residues. Its sequence is as follows:

MENLN MDLLY[10] MAAAV MMGLA[20] AIGAA IGIGI[30] LGGKF LEGAA[40]
RQPDL IPLLR[50] TQFFI VMGLV[60] DAIPM IAVGL[70] GLYVM FAVA[79]

To elucidate the mechanisms underlying H^+-translocation and energy conversion, we employed solid-state NMR (ssNMR) analysis. This is one of the most powerful methods because structural analysis can be performed in a membrane environment. We reported signal assignment for the uniformly [^{13}C, ^{15}N] labeled EF_oc solid with magic-angle spinning (MAS) and estimation of its secondary structure (Kobayashi et al. 2006). A hairpin-like structure was anticipated even in the solid state. Furthermore, we reconstituted the EF_oc oligomer in lipid membranes, and investigated its interaction with lipid bilayers in the liquid-crystalline and gel states (Kobayashi et al. 2008). Characterization of the oligomer strongly suggested that it took on a well-defined ring structure. NMR analysis revealed that the transmembrane-hydrophobic region of the EF_oc oligomer mechanically matched the dipalmitoyl phosphatidylcholine bilayer. The purpose of this work is to characterize the structure of the EF_oc oligomer in membranes and to analyze the ring surface involved in the interaction with the hydrocarbon chains of lipids by ssNMR analysis. Since the structure of the essential acidic residue is not yet well understood in H^+-translocating *c*-rings (Vollmar et al. 2009; Pogoryelov et al. 2009), its structure in the proposed ring models was examined. To obtain reliable information, we have chemically synthesized the whole subunit *c* for site-specific isotope-labeling, and biosynthetically prepared the uniformly ^{13}C, ^{15}N-labeled sample as well. The results have shown that the membrane-reconstituted EF_oc oligomer is similar to the intact *c*-ring in vivo and the structure of the essential residue in the proposed model is unlikely.

Materials and methods

Preparation of uniformly ^{13}C, ^{15}N-labeled subunit *c*

E. coli (MEG119 strain) cells transformed with plasmid pCP35 harboring the EF_o subunit *c* gene were cultured in a ^{13}C- and ^{15}N-labeled CHL medium (CHLORELLA Industry Co., Japan) with a [^{13}C, ^{15}N] amino acid mixture, 0.5 g/l, and [^{13}C] glucose (CIL, Inc., Andover, MA),

4.0 g/l, for 24–26 h. EF_oc was purified according to the reported method (Kobayashi et al. 2006, 2008; Girvin and Fillingame 1993). Subunit *c* was extracted from homogenized cells with 12 wet-cell volumes of a chloroform/methanol (1:1) mixture. The crude subunit *c* was applied to a carboxymethyl cellulose column and eluted with a chloroform/methanol/water (5:5:1) solution. The yield was about 10 mg/4l culture. The purity of the subunit *c* was confirmed by Tricine-SDS–PAGE and MALDI-TOF–MS (Autoflex, Bruker Daltonics, Bremen, Germany).

Chemical synthesis of selectively labeled subunit *c*

EF_oc selectively ^{13}C-labeled at the methyl group of Ala24 and the carboxyl group of Asp61 (EF_oc ([3-^{13}C]Ala24, [4-^{13}C]Asp61)) was chemically prepared by solid phase peptide synthesis based on the Boc (*tert*-butoxycarbonyl group) strategy. Starting from Boc-Ala-OCH_2-Pam resin, a protected peptide corresponding to the sequence of EF_o subunit *c* was assembled with an automated peptide synthesizer, ABI 430A (Applied Biosystems, Foster, CA), except for the two labeled amino acids, which were introduced manually. The protected peptide resin was treated with a mixture of anhydrous HF (9.0 ml) and anisole (1.0 ml) under ice cooling for 90 min, and then HF was evaporated off under reduced pressure. After the residual solid had been washed with ether three times, it was dissolved in trifluoroacetic acid (TFA) and the resin was filtered off. The peptide in the TFA solution was precipitated with ether, suspended in 50% aqueous acetonitrile, and then freeze-dried to give a crude powder. The crude product was purified on a Cosmosil 5PhAR-300 column (10 × 250 mm; Nacalai Tesque, Japan) with a linear gradient of formic acid/water (2:3) and formic acid/1-propanol (4:1) at a flow rate of 2.5 ml/min. The yield of crude EF_o subunit *c* was 3% (w/w). MALDI-TOF MS revealed: *m/z* 8257.6. Calcd for $[M + H]^+$ 8259.1 (average). Amino acid analysis of the synthetic EF_o subunit *c* was performed by hydrolysis with constant-boiling hydrochloric acid at 110°C for 48 h: $Asp_{4.3}Thr_{1.1}Glu_{3.4}Pro_{2.4}Gly_{10}Ala_{12.7}Val_{6.1}Met_{5.7}Ile_{8.0}Leu1_{2.4}$ $Tyr_{1.3}Phe_{4.3}Lys_{0.90}Arg_{2.0}$.

Preparation and characterization of reconstituted membranes

EF_oc was reconstituted into lipid membranes in the same way as reported previously (Kobayashi et al. 2008). 1,2-Diperdeuteriomyristoyl-*sn*-glycero-3-phosphocholine (DMPC-d_{54}) was obtained from Avanti Polar Lipids (Alabaster, AL). Silica gel thin-layer chromatography with development with $CHCl_3$/MeOH/H_2O (65:35:5) gave a single spot. At first, 6 mg of subunit *c* was dissolved in 10 mL of de-ionized water containing about 40 mM octyl-β-D-glucoside (OG) (critical micelle concentration, 25 mM). The solution was visually translucent. Then, DMPC-d_{54} was added to the solution to a protein/lipid molar ratio of 1:40. The mixture was dialyzed for 4 days against 5 l of a buffer solution (200 mM NaCl, 1 mM NaN_3, 10 mM Tris–HCl, pH 8.0) at 26°C, using dialysis tubing with a 8000 molecular weight cutoff (Nacalai Tesque, Inc., Japan). NaCl was omitted from the final dialysis buffer. The reconstituted membranes were collected by centrifugation at 6100 × *g*, and then suspended in 1–2 ml of buffer. To obtain homogeneous liposomes, a freeze–thaw cycle (30, 4, and −30°C for 20 min at each temperature) was repeated more than 10 times. The centrifuged liposomes were put into an NMR rotor. Rotors of 4.0 and 3.2 mmϕ were used for the uniformly labeled and specifically labeled samples, respectively.

Solid-state NMR experiments

NMR measurements were performed with Varian Infinity-plus 500 and 600 spectrometers operating at 11.74 and 14.09 T, respectively (Palo Alto, CA). Broadband double and triple resonance MAS probes for 4.0 and 3.2 mmϕ rotors were used. The MAS frequency was 12.5–13.0 kHz. The probe temperature was set at 193–233 K. The sample temperature could be 10–20°C higher than the probe temperature. Only the probe temperature is given in this paper. The ^1H RF amplitude was 65–75 kHz for TPPM decoupling (Bennett et al. 1995) during the evolution and data acquisition periods, and 70–80 kHz for CW decoupling during the dipolar mixing period. The repetition time was 3 s.

Two-dimensional (2D) ^{13}C homonuclear correlation experiments with DARR (Takegoshi et al. 2001), 2D N–$C^\alpha C^\beta$ correlation experiments (Fujiwara et al. 2004), and a three-dimensional (3D) N–C^α–C' experiment were performed under MAS to obtain the intra-residue correlations. For the inter-residue correlations, 2D N_{i+1}–$(C'C^\alpha)_i$, 2D C^α_{i+1}–$(C'C^\alpha)_i$, and 3D N_{i+1}–C_i'–C^α_i correlation spectra under MAS (Fujiwara et al. 2004) were recorded. For the cross polarization (CP), the RF field amplitude was ramped near the first sideband for the Hartmann-Hahn condition, $\gamma B_1^X = \gamma B_1^H - \omega_R$. Here γB_1^X and γB_1^H are the RF field amplitudes of $^{13}C/^{15}N$ and ^1H, respectively, and ω_R is the sample spinning frequency. The DARR mixing time was 15 ms. The data matrix, 512 (t_1) × 512 (t_2), for DARR was zero-filled to 2048 × 2048. The number of acquisitions was 64 for each FID. Frequency selective CP from ^{15}N to ^{13}C was used in the ^{13}C-^{15}N correlation experiments under the condition of $\gamma B_1^{^{13}C} + \gamma B_1^{^{15}N} = \omega_R$ (Baldus et al. 1998). ^{15}N RF was set at 121 ppm. In the N–$C^\alpha C^\beta$ experiments, the contact time for N/(C^α and C^β) was 4 ms with

$\left(\gamma B_1^{^{13}C}/2\pi, \gamma B_1^{^{15}N}/2\pi\right) = (3\,\text{kHz}, 8\,\text{kHz})$. The data matrix was 216 (t_1) × 512 (t_2) with a spectral width of 50 kHz for both the ^{13}C and ^{15}N axes. For the N_{i+1}–$(C'C^{\alpha}C^{\beta})_i$ pulse sequence, the contact time for N/C′ was 4 ms with $\left(\gamma B_1^{^{13}C}/2\pi, \gamma B_1^{^{15}N}/2\pi\right) = (3\,\text{kHz}, 8\,\text{kHz})$. The DARR mixing time for C′ to $C^{\alpha}C^{\beta}$ was 15 ms with the amplitude of 12.5 kHz. The data matrix was 256 (t_1) × 512 (t_2), and the spectral widths were 60 and 50 kHz for the ^{13}C and ^{15}N axes, respectively. In both N–$C^{\alpha}C^{\beta}$ and N_{i+1}–$(C'C^{\alpha}C^{\beta})_i$ spectra, the data matrices were zero-filled to 1024 × 1024. The numbers of acquisitions for the N–$C^{\alpha}C^{\beta}$ and N_{i+1}–$(C'C^{\alpha}C^{\beta})_i$ experiments were 88 and 128, respectively. In the 3D N_i–C_i^{α} –C_i' experiment, the ^{13}C-^{15}N mixing time was 4 ms with $\left(\gamma B_1^{^{13}C}/2\pi, \gamma B_1^{^{15}N}/2\pi\right) = (9\,\text{kHz}, 4\,\text{kHz})$. The RFDR mixing time for C^{α} to C′ was 1.23 ms with the amplitude of 50 kHz. The spectral widths were 3, 8, and 60 kHz for the ^{15}N, $^{13}C^{\alpha}$, and ^{13}C′ axes, respectively. The data matrix, 15 (t_1) × 37 (t_2) × 512 (t_3), was zero-filled to 128 × 256 × 1024. The number of acquisitions was 64.

In the 2D C_{i+1}^{α}–$(C'C^{\alpha})_i$ pulse sequence, ^{13}C RF was set at 61, 177, and 117 ppm for the two CPs and the RFDR mixing, respectively. ^{15}N RF was set at 120 ppm. The RF amplitudes were $\left(\gamma B_1^{^{13}C}/2\pi, \gamma B_1^{^{15}N}/2\pi\right) = (10\,\text{kHz}, 3\,\text{kHz})$ for C_{i+1}^{α} to N_{i+1}, and $\left(\gamma B_1^{^{13}C}/2\pi, \gamma B_1^{^{15}N}/2\pi\right) = (7\,\text{kHz}, 5\,\text{kHz})$ for N_{i+1} to C_i'. The contact times for C_{i+1}^{α} to N_{i+1} and N_{i+1} to C'_i were 4 ms. The RFDR mixing time was 1.5 ms. The number of acquisitions was 304. The data matrix, 260 (t_1) × 512 (t_2), was zero-filled to 1024 × 1024. In the 3D N_{i+1}–C_i'–C_i^{α} experiment, the ^{13}C–^{15}N mixing time was 4 ms with $\left(\gamma B_1^{^{13}C}/2\pi, \gamma B_1^{^{15}N}/2\pi\right) = (8\,\text{kHz}, 4\,\text{kHz})$. The RFDR mixing time was 1.28 ms with the amplitude of 50 kHz. The spectral widths were 5, 5, and 60 kHz for the ^{15}N, ^{13}C′, and $^{13}C^{\alpha}C^{\beta}$ axes, respectively. The experimental data matrix, 16 (t_1) × 16 (t_2) × 512 (t_3), was zero-filled to 64 × 64 × 1024. The number of acquisitions was 144. The States method was used for quadrature detection in the indirect dimension. Measurements so far were carried out at 14.09 T and 233 K.

^{13}C-NMR observation of ^{2}H-selective ^{1}H-depolarization (CODSHD) under MAS was carried out at 223 K and 11.74 T according to the reported method (Harada et al. 2006). The RF phase for the depolarization period was alternated at the interval of 200 ms for ^{2}H. The ^{1}H depolarization was facilitated by phase-alternating cross polarization. The flip angle of all the ^{1}H pulses was 54.7°. The B_1 field amplitudes satisfy the condition $\gamma B_{1,X} = \gamma B_{1,1H}^{\text{eff}} - \omega_R$ mentioned above at the spinning rate of 10 kHz. The $B_{1,X}$ amplitudes were 42 kHz for ^{2}H and 77 kHz for ^{13}C. The frequency of B_1 was shifted by about 150 kHz under the off Hartmann-Hahn condition. The contact time for ^{13}C-^{1}H Lee-Goldburg cross polarization (LGCP) was 100 μs. The ^{1}H RF amplitude was 70 kHz. 24,000 transients were accumulated.

A rotational resonance (RR) experiment under MAS for the EF_o Ala24 [$^{13}C^{\beta}$], Asp61 [$^{13}C^{\gamma}$]-subunit *c* was performed at ν_R of 12.155 kHz under the $n = 2$ RR condition. The temperature and magnetic field were 193 K and 14.09 T, respectively. A constant-time rotational resonance pulse sequence (Balazs and Thompson 1999) was used to suppress the evolution time-dependent sample heating by the RF fields. Spectra of the natural abundance and labeled EF_oc were obtained with the same evolution time for evaluation of the magnetization transfer.

The obtained FID signals were processed with Felix2007 (Felix NMR Inc., San Diego, CA). Fourier-transformations were performed with exponential and sine-bell broadening functions. The ^{13}C chemical shift was referenced to DSS by using the methine carbon signal of adamantane under MAS at 40.5 ppm relative to DSS (Morcombe and Zilm 2003). The ^{15}N chemical shift was referenced to that of liquid NH_3 deduced from the ^{13}C chemical shift using the $\gamma^{^{15}N}/\gamma^{^{13}C}$ ratio following the IUPAC recommendation (Markley et al. 1998).

An EF_oc decamer model mimicking the crystal structure of IF_oc-ring

The crystal structure of the IF_oc-ring (PDB ID, 1yce) was used as the starting structure. Sequential alignment was carried out with Visual Molecular Dynamics 1.8.6 (Humphrey et al. 1996). Then, amino acid residues were replaced, using SCWRL Server (http://www1.jcsg.org/scripts/prod/scwrl/serve.cgi) (Canutescu et al. 2003). Finally, the decamer structure was optimized with Xplor-NIH 2.13 (Schwieters et al. 2003) under the restrictions of inter-subuint C^{α}-C^{α} distances of the IF_oc-ring, and dihedral angles and inter-helix C^{α}-C^{α} distances of the EF_oc solution structure (PDB ID, 1c99).

Results

Secondary structure information on the EF_oc in DMPC membranes

It was confirmed in our previous work that well-defined EF_oc oligomers could be reconstituted in DMPC membranes (Kobayashi et al. 2008). To obtain secondary structure information on EF_oc, we recorded solid-state NMR spectra for it. Figure 1 presents 2D ^{13}C–^{13}C DARR spectra of the uniformly ^{13}C-labeled EF_o subunit *c*/DMPC bilayers. Since EF_oc is an integrated membrane protein, it

contains 13 Ala, 12 Leu, 10 Gly, 8 Met, 8 Ile, and 6 Val residues, which account for 72% of the 79 residues. This causes serious signal overlapping. The DARR dipolar mixing provided cross peaks among aliphatic carbons (Fig. 1), among aromatic carbons (data not shown), and between the aromatic and C^{β} carbons of Phe and Tyr (data not shown). The spectrum was similar to that of the uniformly ^{13}C-labeled EF_o subunit *c* solid without lipids (Kobayashi et al. 2006). However, the resolution of $C^{\alpha\beta}$ cross peaks in the spectrum is much better than that reported, revealing that the EF_oc structure is homogeneous in membranes. This is consistent with the results of ultracentrifugation analysis (Kobayashi et al. 2008). To check the resolution, we compared the $Val^{\alpha\beta}$ cross peaks that appeared on opposite sides of a diagonal line (in boxes), as shown at the bottom of Fig. 1. There are at least three resolved signals with a line-width of 1 ppm. However, there are differences of up to 0.5 ppm in the peak tops except for that of the peak at around (66.7, 31.7) ppm due to the effect of noise. The intra-residue spin connectivities of major Ala, Leu, Val and Ile residues can be traced, as shown in Fig. 1. The cross peaks of their side chains are not resolved, in contrast to those of $C^{\alpha\beta}$. The C^{α}/C^{β} chemical shifts of the EF_oc subunit monomer in an organic solution (Girvin et al. 1998) are presented in the figure as red dots. They overlap with the corresponding cross peaks of EF_oc in membranes, suggesting that the major secondary structures of EF_oc in membranes are similar to the solution structure. However, there are also some clear differences. To obtain more detailed information, we carried out partial assignment of the ^{13}C and ^{15}N signals. The details of this are given in the supporting material.

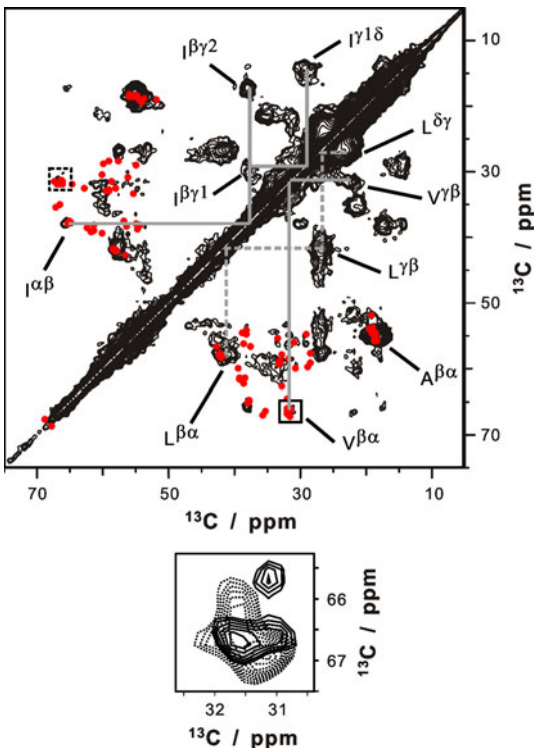

Fig. 1 Intra-residue 2D ^{13}C-^{13}C correlation DARR spectrum of [U-^{13}C, ^{15}N] EF_o subunit *c* in d_{54}-DMPC bilayers (EF_oc/DMPC). The DARR mixing time was 15 ms. The carbon spin systems of Leu, Val and Ile were connected, respectively. A sine-bell window function (90°) was used. *Red cross peaks* are the chemical shifts obtained for EF_oc in solution (Girvin et al. 1998). *Bottom*, superimposed Val $C^{\alpha\beta}$ cross peaks in two symmetric regions (*in boxes*)

A 2D ^{13}C–^{15}N spectrum for the intra-residue N–C^{α} correlation (Fig. S1*A*) provided the information on Pro cross peaks at (64.7, 137) and (62.3, 134) ppm. Two pieces of sequential information could be obtained from a 2D ^{13}C–^{15}N spectrum for the N_{i+1}–$(C'C^{\alpha}C^{\beta})_i$ correlation (Fig. S1*B*). The isolated cross peak of G32G33 can be easily identified. The cross peak at (55.5, 134) ppm can be assigned to Q42P43 because of the Pro-specific ^{15}N chemical shift and its $^{13}C^{\alpha}$ chemical shift, excluding the possibility of two other Pro residues (I46P47 and I63P64).

We have carried out further assignment on the basis of inter-residue C^{α}_{i+1}-C^{α}_i correlations. Here, we could convert the shortcoming of the membrane protein to an advantage. Namely, the C^{α} signals of Gly, Ile, and Val residues, which are the main components of membrane proteins, could be efficiently used for the assignment because of their significantly high or low field shifts. Figure 2 presents an inter-residue C^{α}_{i+1}-C^{α}_i correlation spectrum of EF_oc/DMPC bilayers. Although the central part of the spectrum is congested, we can take advantage of the isolated cross peaks for sequential assignment. Furthermore, the chemical shift of a certain amino acid residue was assumed to be in the range of the average chemical shift ±2x(standard deviation) in BMRB database. This covers 95% of the deposited data, assuming their Gaussian distribution. For example, when we start from a unique sequence, G32G33, sequential walking from I28 to K34 can be performed, as shown in Fig. 2. L31G32 should be at (58.5, 47.5) ppm, since the other possibility at around (60, 47.5) ppm does not exhibit connectivity with I30L31. Otherwise, the connectivity is straightforward. In addition to this, sequential walking for A21 ~ I28, E37 ~ A39, I55 ~ L59, A67 ~ L72, and F76 ~ V78 could be carried out, as discussed in the supporting material (Fig. S2), leading to the assignment of 36 C^{α} signals in total.

Analysis of the intra- and inter-residue 3D spectra provided the chemical shifts of ^{15}N and carbonyl ^{13}C. An example of 3D sequential walking for A67-Y73 is presented in Fig. S1*C*. The obtained chemical shifts are summarized in Table S1 in the supporting material and deposited with BMRB (ID 11172). The dihedral angles of

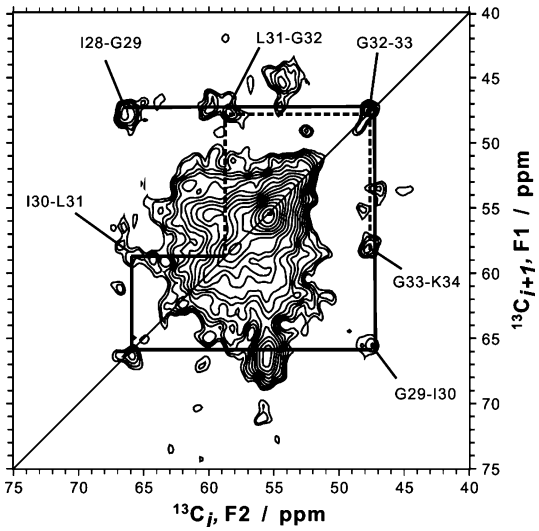

Fig. 2 2D C^{α}_{i+1}-C^{α}_{i} correlation spectrum of [U-^{13}C, ^{15}N] EF_oc/DMPC. Sequential walking for the region from I28 to K34 is presented, as an example. Additional walking is presented in the supplemental figures. An exponential window function with 100 Hz broadening factor was used

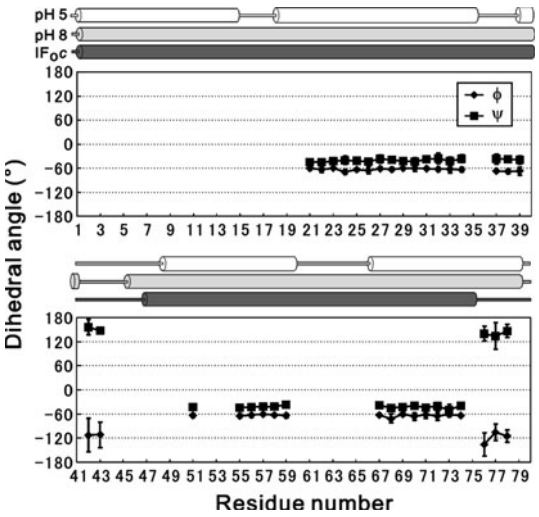

Fig. 3 Predicted backbone dihedral angles of EF_oc in membranes. The dihedral angles, ϕ and ψ, were predicted with TALOS, using the chemical shifts in Table S1. The *error bars* indicate RMSD for the ten predicted dihedral angles. The secondary structures of EF_oc in an organic solvent at pH 5 and 8 (Girvin et al. 1998; Rostogi and Girvin 1999), and those in the Na^+-ATPase crystal structure (IF_oc) (Meier et al. 2005) are also presented on the *top* by *rods* (helices) and *sticks* (extended)

the main chain were deduced from the chemical shifts of the assigned signals with program TALOS (Cornilescu et al. 1999), and are presented as a function of the sequence in Fig. 3. The angles indicate an α-helical conformation except for the Q42 ∼ P43 and F76 ∼ V78 regions.

Magnetization transfer from protons of the subunit *c* to deuterons of the lipid membrane

To examine the exposure of amino acid residues to membrane lipids, we measured the magnetization transfer between the protons of subunit *c* and the deuterons of fatty acid chains in EF_oc/d_{54}-DMPC bilayers by means of ^{13}C-NMR observation of ^{2}H-selective ^{1}H-depolarization (CODSHD) pulse sequence with MAS (Harada et al. 2006). The results are presented in Fig. 4, the contact times being on the right. The reference spectrum at the top was obtained with the Lee-Goldburg cross polarization (LGCP) pulse sequence (Lee and Goldburg 1965). It contains all ^{13}C signals expected for that of EF_oc. The others are difference spectra, exhibiting only CODSHD signals. Therefore, the residues giving rise to these signals should be located on the surface close to the hydrocarbon chains of the lipids. The signals derived from hydrocarbon chains are suppressed by deuteration.

While the CODSHD spectra with different contact times are similar to one another, their spectral patterns are significantly different from that of LGCP. In the former, sharp peaks at 14.2 (shoulder), 17.6, 47.5 and 65.8 ppm are clearly enhanced, suggesting that specific amino acid residues are involved in magnetization transfer. In addition, observed is a broad aromatic peak at around 130 ppm, which can be assigned to Phe, because of the weak pure

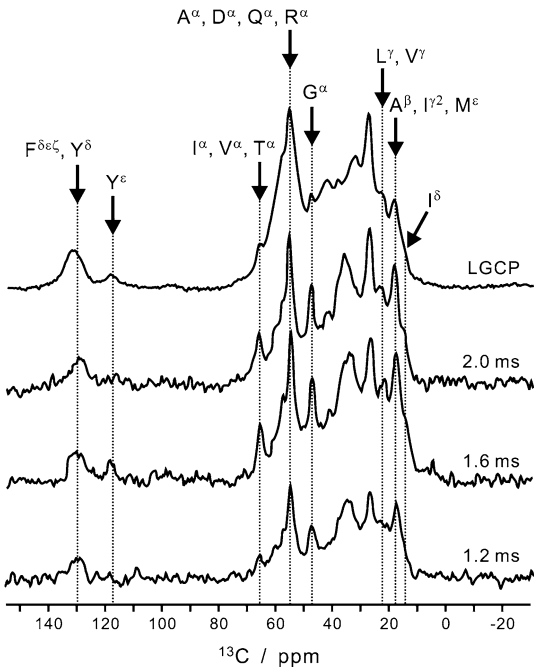

Fig. 4 ^{2}H-selective ^{1}H-depolarization ^{13}C-NMR (CODSHD) spectra of [U-^{13}C, ^{15}N] EF_oc/d_{54}-DMPC bilayers. Contact times are given on the *right*. The LGCP spectrum is a reference one. Amino acid residues that may contribute to each peak are indicated with a *single-letter code*. Line broadening, 150 Hz

Tyr C^{ε} signal at around 118 ppm. Among the enhanced, the peak at 47.5 ppm can be assigned to Gly C^{α}, because there is no cross peaks at around this chemical shift in spite of the presence of a diagonal peak in the DARR spectrum (Fig. 1). The shoulder at 14.2 ppm can be assigned to Ile C^{δ}, because no other signals appear in this region (Fig. 1). Consequently, at least one Phe, one Ile, and one Gly are located on or close to the surface facing the hydrophobic region of lipids.

Measurement of the distance between Ala24 C^{β} and Asp61 C^{γ} in the EF_oc-oligomer

It was shown that an acidic amino acid residue plays an essential role in the proton translocation across membrane (Fillingame 1992). This is Asp61 in EF_oc. Furthermore, EF_oc mutant proteins with interchange of Asp61 and Ala24 (A24D/D61G or A24D/D61 N EF_oc) were found not to impair the activity of EF_oF_1 (Fillingame and Dmitriev 2002). Therefore, these residues should be closely correlated in the subunit *c*-ring. Actually, in the proposed models of the EF_o subunit *c*-ring for the decamer and dodecamer, the distances between Ala24 C^{β} and Asp61 C^{γ} are 0.42 and 0.44 nm, respectively (Jiang et al. 2001). Since this information is important to examine a structural model of the *c*-ring, we chemically synthesized EF_oc ([3-^{13}C]Ala24, [4-^{13}C]Asp61), using a solid-phase peptide synthesis method developed for this study. The specifically labeled EF_oc was reconstituted into deuterated DMPC membranes. The rotational resonance (RR) was observed at different mixing times (0.01, 5, 10, 15, and 20 ms). The results are presented in Fig. 5. To make the comparison clear, the intensity differences between the labeled and natural abundant ones are only presented for the Ala24 $^{13}C^{\beta}$ and Asp61 $^{13}C^{\gamma}$ signals of EF_oc. As can be seen in the figure, there was no intensity change for the mixing times examined. Actually, a clear decay of the magnetization transfer was observed for the distance of 0.42 nm in the case of membrane-bound Mastoparan X with the same machine under the same conditions (Todokoro et al. 2006). Similar observations were reported for RR experiments on Neu receptor tyrosine kinase (Smith et al. 2002), Ca^{2+}-ATPase (Hughes and Middelton 2003), and others. On the basis of analysis, the distance between Ala24 C^{β} and Asp61 C^{γ} should be greater than 0.6 nm.

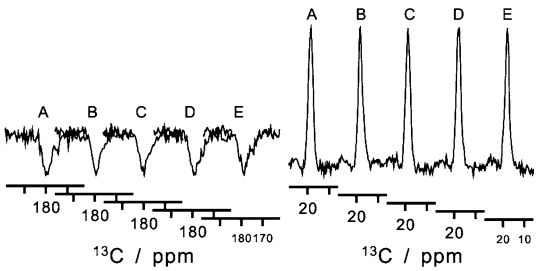

Fig. 5 ^{13}C rotational resonance spectra of EF_oc ([3-^{13}C]Ala24, [4-^{13}C]Asp61)/DMPC as a function of the mixing time. Resonance conditions, $n = 2$ at $\nu_R = 12.155$ kHz. Only the methyl and carboxyl carbon signals of the labeled/non-labeled difference spectrum are presented. The mixing times for spectra *A*, *B*, *C*, *D*, and *E* were 0.01, 5, 10, 15, and 20 ms, respectively. Line broadening, 50 Hz

We could also determine the chemical shifts of Ala24 C^{β} and Asp61 C^{γ} unequivocally from the spectra. The chemical shift of the latter is 179.6 ppm. Since the chemical shifts of the protonated and deprotonated carboxyl carbons are 179.5 and 180.7 ppm, respectively (Smith et al. 1996), the side chain of Asp61 should take on the protonated (COOH) state.

Discussion

The EF_oc oligomers in octylglucoside micelles were found to be homogeneous by ultracentrifuge analysis and the reconstituted EF_oc/DMPC-liposomes gave rise to a single band on sucrose density gradient analysis (Kobayashi et al. 2008). On the basis of these results and earlier reports (Dmitriev et al. 1995; Arechaga et al. 2002), we assumed that EF_oc oligomers reconstituted in DMPC bilayers take on a ring structure similar to the intact one (Kobayashi et al. 2008). Observation of a single set of signals in the spectra is consistent with the rotational symmetry of the ring structure. We carried out all experiments at −40, −50 or −80°C to obtain well-defined structural information.

Figure 3 reveals that the region of A21 ∼ A39 in the N-terminal half, and those of I55 ∼ L59 and A67 ∼ V74 in the C-terminal half take on α-helical conformations. In addition to the information derived from sequence-specific dihedral angles, amino acid-specific chemical shifts also provide the secondary structure information. In the M1 ∼ A20 region, four Ala and four Leu residues are located. Most of them must take on α-helical conformations in view of DARR spectrum in Fig. 1. Therefore, the major part of the N-terminal half would take on an α-helical conformation like in the case of the solution EF_oc structures and the IF_oc crystal structure (Fig. 3, top). In the C-terminal half, there are three Leu and one Ile residue, and one Ala and two Ile residues in the L45 ∼ R50 and V60 ∼ I66 regions, respectively, suggesting that the major part of the C-terminal half also takes on an α-helical conformation. In contrast, Q42P43 take on an extended conformation. These two residues comprise a conserved sequence in loop structures in the known hairpin structures. Consequently, each EF_oc in the oligomer would take on a hairpin-type helix-loop-helix conformation in membranes

as in solution (Girvin et al. 1998; Rastogi and Girvin 1999). The CODSHD and RR experiments provided more detailed information on the EF_oc-oligomer structure.

Regarding the magnetization transfer with CODSHD, we have to consider the contributions of deuteron reservoirs inside and outside of the ring. Most of DMPC molecules are located outside of the *c*-ring. However, they may reside inside of the ring as well, although there is no direct evidence so far. According to molecular dynamics estimation, about six PC molecules can be accommodated the inner space (Dr. S. Fuchigami, personal communication). Taking the ratio of $PC/EF_oc = 40$ into account, the ratio of PC_{out}/PC_{in} is 66. On the other hand, the ratio of the outer and inner surfaces is about ten. This should be correlated to the deuteron density ratio at the two surfaces. Therefore, the contribution of the signals from the inner surface is about one-tenth of that of those from the outer surface at a short contact time. This will gradually decrease to 1/66 along with an increase in the contact time. Because of the contact-time independency of the spectral pattern, the enhanced peaks in Fig. 4 can be attributed to the outer surface of the ring. This is the case with at least one Gly, one Phe and one Ile residue. In the N-terminal helix, there is only one Phe in the sequence K^{34}FLEGAA. Since this region is polar and is a direct neighbor of the loop, it should be in the polar-head area in the membrane. Therefore, Phe35 would not contribute to CODSHD. In the C-terminal helix, there are three Gly, three Phe and four Ile in the hydrophobic region. We can assume a pitch of roughly 3.6 residues/turn for a helix. Thus, the following line-ups on the surface across a membrane are possible, assuming 60° allowance around the helix axis: Namely, (a) V56, (L59V60), I63, (I66A67), L70, and (Y73V74), (b) (F53F54), M57, (V60D61), P64, (A67V68), G71, and (V74M75), (c) (F54I55), G58, (D61A62), M65, (V68G69), and L72, (d) (I55V56), L59, (A62I63), I66, (G69L70), and Y73, (e) F53, (V56M57), V60, (I63P64), A67, (L70G71), and V74, (f) F54, (M57G58), D61, (P64M65), V68, (G71L72), and M75, and (g) I55, (G58L59), A62, (M65I66), G69, (L72Y73), and F76. Here, the single residue is assumed to fall on the line-up, and the residues in a parenthesis are assumed to be located around the line connecting single residues in each line-up. Only line-ups (c), (e) and (g) include a combination of Gly, Phe, and Ile. In the cases of (c) and (e), however, there are two issues, which contradict with the observation. First, although signals due to Val and Leu should be enhanced in these cases, the signal at around 23 ppm due to Val and Leu is not enhanced. Second, although a weak Tyr signal is observed at around 118 ppm, line-ups (c) and (e) do not include Tyr. Therefore, (c) and (e) are unlikely. If (g) is the case, Ala signals should be enhanced in addition to Ile, Gly, and Phe. The intense CODSHD signals at around 18 and 55 ppm are consistent with this requirement. Therefore, we can conclude that line-up (g) is located on the outer surface of the EF_oc-ring.

The accessibility of the amino acid residues of EF_oc to EF_o subunit *a* has been extensively investigated by means of cross-linking methods (Moore and Fillingame 2008; Jiang and Fillingame 1998). Our observation can be directly compared with the results. The cross-linking experiments revealed that Phe54, Ile55, Ala62, Met65, Gly69, Leu72 and Tyr73 were accessible to residues on subunit *a* (Jiang and Fillingame 1998). Therefore, they should be located on the outer surface of the *c*–ring. This coincides with our conclusion rearding Ile55, Ala62, and Gly69. In addition, Met65, Leu72 and Tyr73 should also be located on the surface area as shown in the parentheses. Phe76 was not examined in the cross-linking experiment. Furthermore, the I55C mutation completely suppressed growth, and the G69C and Y73C ones resulted in significantly low growth (Jiang and Fillingame 1998), suggesting the importance of these residues. The agreement of our observation on magnetization transfer with the cross-linking between subunits *a* and *c* in vivo substantiates our assumption that EF_o subunits *c* in DMPC bilayers form a ring structure similar to the intact one in *E. coli* membranes.

This agreement allows us to evaluate the proposed model structures for the EF_oc-ring, using the results of our RR experiment. It turned out from the crystal structures of *c*-rings (Vollmar et al. 2009; Pogoryelov et al. 2009) that the structure around the essential amino acid could be different for different species. Therefore, it is important to examine the structure of Asp61 in the EF_oc-ring in a membrane. It was revealed in this work that the distance between Ala24 C^{β} and Asp61 C^{γ} is longer than 0.6 nm, while the distances in the decamer and dodecamer models of the EF_oc-ring structures (PDB ID, 1J7F) are around 0.44 and 0.42 nm, respectively (Fig. 6A, B). Therefore, our results are not consistent with the current models. There are four reported structures of subunit c-rings (Stock et al. 1999; Vollmar et al. 2009; Pogoryelov et al. 2009; Meier et al. 2005). Among them, IF_oc_{11} (Meier et al. 2005) is closest to the EF_oc-ring in terms of the subunit number. The distance corresponding to Ala24 C^{β} and Asp61 C^{γ} in the EF_oc-ring is that of Pro29 C^{β}-Glu68 C^{γ} in IF_oc. It is 0.57 nm, as shown in Fig. 6C. Since Glu68 in IF_oc is coordinated to Na^+, we should focus our attention on the global orientation of the side chain. As can be seen in Fig. 6, the orientation of the essential acidic amino acid is different for the EF_oc model and the IF_oc-ring crystal structure in terms of the helix rotation and packing. On the basis of our distance analysis, the helix packing of IF_oc might be better than that of the EF_oc-ring model. We built an EF_oc decamer model based on the crystal structure of IF_oc-ring (see "Materials and methods"). In this model, Ile55, Ala62, and Gly69 are lined up on the surface of the

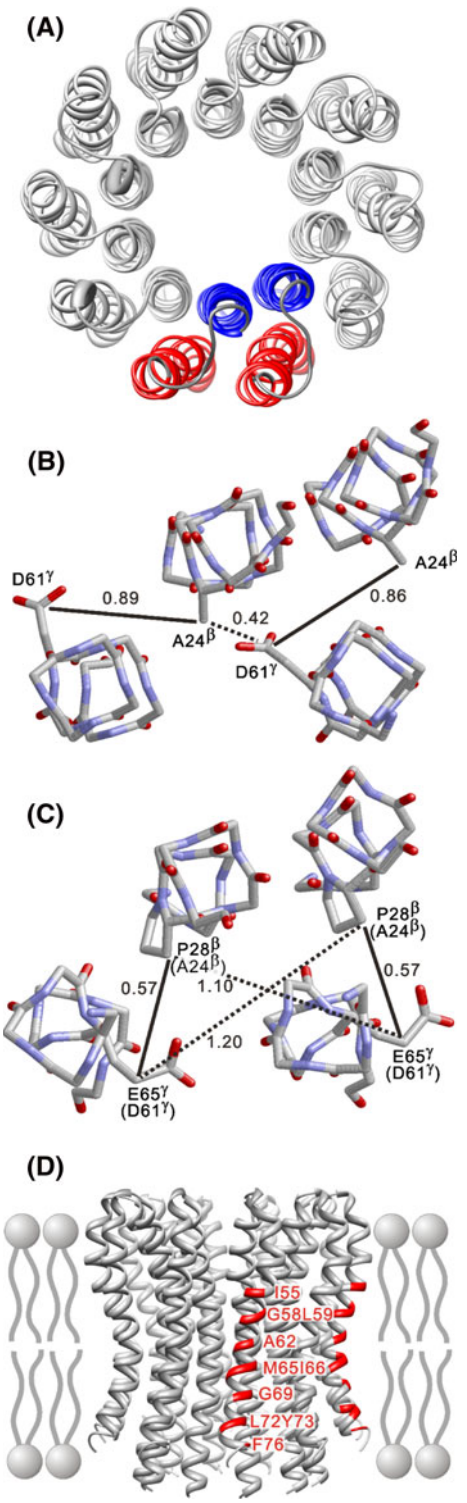

◀**Fig. 6** Model structures of the EF_oc decamers, the distance between Ala24 C^{β} and Asp61 C^{γ} in the model, and the corresponding one in the IF_oc-ring structure. The *helices* are viewed from the polar loop end of the subunit *c* hairpin in **A**, **B** and **C**. **A** A *top view* of the EF_oc decamer-ring model (Jiang et al. 2001); **B** a blowup of the relevant region of the two subunits colored in **A**; **C** the corresponding region in the IF_oc-ring structure (PDB ID, 1yce); and **D** a model structure of EF_oc decamer mimicking the crystal structure of IF_oc-ring. The residues in the line-up derived from the CODSHD spectra (Fig. 4) are colored *red*. The *solid and broken lines* are intra- and inter-molecule distances, respectively. The models in **A** and **D**, and **B** and **C** were drawn using UCSF CHIMERA (Pettersen et al. 2004) and RASMOL (Sayle and Milner-White 1995), respectively

ring as can be seen in Fig. 6D. The shortest distance between Ala24 C^{β} and Asp61 C^{γ} (corresponding to the solid line in Fig. 6C) is about 6.5 nm in good agreement with our observation. However, the structural determination is left for the future. Furthermore, it is important to point out that the protonated state of the Asp61 carboxyl group is stabilized in the *c*-ring even at neutral pH.

It was shown in our previous work that EF_oc-rings hydrophobically and mechanically match the DMPC bilayers in the liquid-crystalline state (Kobayashi et al. 2008). Namely, perturbation of a subunit *c*-ring on hydrocarbon chains is subtle in contrast to in the cases of other membrane proteins. This would be important for smooth rotation of the subunit *c*-ring in membranes coupled with H^+ translocation. The CODSHD experiment has revealed that Ile55, Ala62, Gly69, and Phe 76 are located on the hydrophobic surface. This means that residues with relatively small side chains appear on the surface in the central region of a membrane as can be seen in Fig. 6D. The smaller side chains provide more space in the center, which supports the motions of the methyl terminal regions of hydrocarbon chains of lipids and longer side chains of subunits *c* on the surface. Thus, the hydrocarbon chains of lipids would be able to interact with the surface of the subunit *c*-ring without stress.

In conclusion, the assigned chemical shifts suggest that EF_oc in a membrane takes on a hairpin-type helix-loop-helix conformation in the *c*-ring. The magnetization transfer results coincide with those of the cross-linking experiments, which substantiates that the EF_oc ring structure in DMPC membranes is similar to the intact one built in H^+-ATP synthase in *E. coli* membranes. The distance measurement was not consistent with the proposed EF_oc-ring models. In the ring structure, the side chain of essential Asp61 takes on the COOH state. The hydrophobic surface of the EF_oc-ring carries relatively small side chains in its central region, which may allow soft and smooth interactions with the hydrocarbon chains of lipids in the liquid-crystalline state.

Acknowledgments We are grateful to Profs. R. H. Fillingame and M. Yoshida for providing us with the *E. coli* MEG119 strain transformed with plasmid pCP35 harboring the gene of subunit *c* from *E. coli* and for their encouragement. We also thank Mr. Y. Hayakawa for his help in analysis of the spectra. This work was partly supported by the Target Protein Program (HA, TF, and SA), Grants-in-Aid for Scientific Research on Priority Areas from the Ministry of Education, Science, Technology, Sport and Culture of Japan (HA and SA), and a WCU Grant from Korean Research Foundation funded by Korea government, MEST (HA).

References

Arechaga I, Butler PJG, Walker JE (2002) Self-assembly of ATP synthase subunit *c* rings. FEBS Lett 515:189–193

Balazs YS, Thompson LK (1999) Practical methods for solid-state NMR distance measurements on large biomolecules. J Magn Reson 139:371–376

Baldus M, Petkova AT, Herzfeld J, Griffin RG (1998) Cross polarization in the tilted frame: assignment and spectral simplification in heteronuclear spin systems. Mol Phys 95:1197–1207

Bennett AE, Rienstra CM, Auger M, Lakshmi KV, Griffin RG (1995) Heteronuclear decoupling in rotating solids. J Chem Phys 103:6951–6958

Boyer PD (1997) The ATP synthase—a splendid molecular machine. Annu Rev Biochem 66:717–749

Canutescu AA, Shelenkov AA, Dunbrack RJ Jr (2003) A graph theory algorithm for protein side-chain prediction. Protein Sci 12:2001–2014

Cornilescu G, Delaglio F, Bax A (1999) Protein backbone angle restraints from searching a database for chemical shift and sequence homology. J Biomol NMR 13:289–302

Dimroth P, Von Ballmoos C, Meier T (2006) Catalytic and mechanical cycles in F-ATP synthase. EMBO Rep 7:276–282

Dmitriev OY, Altendorf K, Fillingame RH (1995) Reconstitution of the F_o complex of *Escherichia coli* ATP synthase from isolated subunits. Eur J Biochem 233:478–483

Dmitriev OY, Jones PC, Fillingame RH (1999) Structure of the subunit *c* in the F_1F_o ATP synthase: model derived from solution structure of the monomer and cross-linking in the native enzyme. Proc Natl Acad Sci USA 96:7785–7790

Fillingame RH (1992) H^+ transport and coupling by the F_o sector of the ATP synthase: insights into the molecular mechanism of function. J Bioenerg Biomembr 24:485–491

Fillingame RH, Dmitriev OY (2002) Structural model of the transmembrane F_o rotary sector of H^+-transporting ATP synthase derived by solution NMR and intersubunit cross-linking in situ. Biochim Biophys Acta 1565:232–245

Fujiwara T, Todokoro Y, Yanagishita H, Tawarayama M, Kohno T, Wakamatsu K, Akutsu H (2004) Signal assignments and chemical-shift structural analysis of uniformly ^{13}C, ^{15}N-labeled peptide, mastoparan-X, by mutidimensional solid-state NMR under magic-angle spinning. J Biomol NMR 28:311–325

Girvin ME, Fillingame RH (1993) Helical structure and folding of subunit *c* of F_1F_o ATP synthase: ^1H NMR resonance assignments and NOE analysis. Biochemistry 32:12167–12177

Girvin ME, Rastogi VK, Abildgaard F, Markley JL, Fillingame RH (1998) Solution structure of the transmembrane H^+-transporting subunit *c* of the F_1F_o ATP synthase. Biochemistry 37:8817–8824

Harada E, Todokoro Y, Akutsu H, Fujiwara T (2006) Detection of peptide- phospholipid interaction sites in bilayer membranes by ^{13}C NMR spectroscopy: observation of ^2H, ^{31}P-selective ^1H-depolarization under magic-angle spinning. J Am Chem Soc 128:10654–10655

Hughes E, Middelton DA (2003) Solid-state NMR reveals structural changes in phospholamban accompanying the functional regulation of Ca^{2+}-ATPase. J Biol Chem 278:20835–20842

Humphrey W, Dalke A, Schulten K (1996) VMD: visual molecular dynamics. J Mol Graph 14:33–38

Hutcheon ML, Duncan TM, Ngai H, Cross RL (2001) Energy-driven subunit rotation at the interface between subunit a and the c oligomer in the F_o sector of *Escherichia coli* ATP synthase. Proc Natl Acad Sci USA 98:8519–8524

Jiang W, Fillingame RH (1998) Interacting helical faces of subunits *a* and *c* in the F_1F_o ATP synthase of *Escherichia coli* defined by disulfide cross-linking. Proc Natl Acad Sci USA 95:6607–6612

Jiang W, Hermolin J, Fillingame RH (2001) Preferred stoichiometry of *c* subunits in the rotary motor sector of *Escherichia coli* ATP synthase is 10. Proc Natl Acad Sci USA 98:4966–4971

Kobayashi M, Matsuki Y, Yumen I, Fujiwara T, Akutsu H (2006) Signal assignment and secondary structure analysis of a uniformly [^{13}C, ^{15}N]-labeled membrane protein, H^+-ATP synthase subunit *c*, by magic-angle spinning solid-state NMR. J Biomol NMR 36:279–293

Kobayashi M, Struts AV, Fujiwara T, Brown MF, Akutsu H (2008) Fluid mechanical matching of H^+-ATP synthase subunit *c* ring with lipid membranes revealed by ^2H solid-state NMR. Biophys J 94:4339–4347

Lee M, Goldburg WI (1965) Nuclear-magnetic-resonance line narrowing by a rotating rf field. Phys Rev 140:A1261–A1271

Markley JL, Bax A, Arata Y, Hilbers CW, Kaptein R, Sykes BD, Wright PE, Wüthrich K (1998) Recommendations for the presentation of NMR structures of proteins and nucleic acids. Pure Appl Chem 70:117–142

Meier T, Polzer P, Diederichs K, Welte W, Dimroth P (2005) Structure of the rotor ring of F-type Na^+-ATPase from *Ilyobacter tartaricus*. Science 308:659–662

Moore K, Fillingame RH (2008) Structure interactions between transmembrane helices 4 and 5 subunit *a* and the subunit *c* ring of *Escherichia coli* ATP synthase. J Biol Chem 283:31726–31735

Morcombe CR, Zilm KW (2003) Chemical shift referencing in MAS solid state NMR. J Magn Reson 162:479–486

Murata T, Yamato I, Kakinuma Y, Leslie AG, Walker JE (2005) Structure of the rotor of the V-type Na^+-ATPase from *Enterococcus hirae*. Science 308:654–659

Nakano T, Ikegami T, Suzuki T, Yoshida M, Akutsu H (2006) A new solution structure of ATP synthase subunit *c* from thermophilic *Bacillus* PS3, suggesting a local conformational change for H^+-translocation. J Mol Biol 358:132–144

Pettersen EF, Goddard TD, Huang CC, Couch GS, Greenblatt DM, Meng EC, Ferrin TE (2004) UCSF Chimera—a visualization system for exploratory research and analysis. J Comput Chem 25:1605–1612

Pogoryelov D, Yildiz Ö, Faraldo-Gómez JD, Meier T (2009) High-resolution structure of the rotor ring of a proton-dependent ATP synthase. Nat Struct Mol Biol 16:1068–1073

Rastogi VK, Girvin ME (1999) Structural changes linked to proton translocation by subunit c of the ATP synthase. Nature 402:263–268

Sayle RA, Milner-White EJ (1995) RASMOL: biomolecular graphics for all. Trends Biochem 20:374–376

Schwieters CD, Kuszewski JJ, Tjandra N, Clore GM (2003) The Xplor-NIH NMR molecular structure determination package. J Magn Reson 160:65–73

Smith SO, Smith CS, Bormann BJ (1996) Strong hydrogen bonding interactions involving a buried glutamic acid in the transmembrane sequence of the neu/erbB-2 receptor. Nat Struct Biol 3:252–258

Smith SO, Smith C, Shekar S, Peersen O, Ziliox M, Aimoto S (2002) Transmembrane interactions in the activation of the Neu receptor tyrosine kinase. Biochemistry 41:9321–9332

Stock D, Leslie AG, Walker JE (1999) Molecular architecture of the rotary motor in ATP synthase. Science 286:1700–1705

Suzuki T, Ueno H, Mitome N, Suzuki J, Yoshida M (2002) F_o of ATP synthase is a rotary proton channel. J Biol Chem 277:13281–13285

Takegoshi K, Nakamura S, Terao T (2001) 13C–1H dipolar-assisted rotational resonance in magic-angle spinning NMR. Chem Phys Lett 344:631–637

Todokoro Y, Yumen I, Fukushima K, Kang SW, Park JS, Kohno T, Wakamatsu K, Akutsu H, Fujiwara T (2006) Structure of tightly

membrane-bound mastoparan-X, a G-protein-activating peptide, determined by solid-state NMR. Biophys J 91:1368–1379

Vollmar M, Schlieper D, Winn M, Büchner C, Groth G (2009) Structure of the c_{14} rotor ring of the proton translocating chloroplast ATP synthase. J Biol Chem 284:8228–18235

Yoshida M, Muneyuki E, Hisabori T (2001) ATP synthase—a marvellous rotary engine of the cell. Nat Rev Mol Cell Biol 2:669–677